PAPER

NJC
www.rsc.org/njc

Absorption and solvatochromic properties of 2-methylisoindolin-1-one and related compounds: interplay between theory and experiments

Fabien Gutierrez,[a] Jérôme Trzcionka,[b] Rodolphe Deloncle,[b] Romuald Poteau[a] and Nadia Chouini-Lalanne[b]

[a] *Laboratoire de Physique Quantique (CNRS UMR 5626), IRSAMC, Université Paul Sabatier, 118 route de Narbonne, 31062 Toulouse cedex, France. E-mail: romuald.poteau@irsamc.ups-tlse.fr*

[b] *Laboratoire des Interactions Moléculaires et Réactivité Chimique et Photochimique (CNRS UMR 5623), Université Paul Sabatier, 118 route de Narbonne, 31062 Toulouse cedex, France. E-mail: lalanne@chimie.ups-tlse.fr*

Received (in Montpellier, France) 13th October 2004, Accepted 30th November 2004
First published as an Advance Article on the web 24th February 2005

The excited states of 2-methylisoindolin-1-one (INS) have been investigated by absorbance spectroscopy and theoretical calculations performed at the TDDFT level and compared with those of three related compounds involved in DNA photosensitization: indanone (IND), indoprofen (INP), a nonsteroidal anti-inflammatory drug and one of the INP photoproducts, the 2-(4-acetylphenyl)isoindolin-1-one (KINP), in order to understand the influence of the nitrogen atom and of substitutions on the lowest singlet excited states of the isoindolinone chromophore. TDDFT calculations combined with a polarizable continuum model (PCM) reproduced fairly well the experimental spectra and the solvatochromism. The study of the molecular orbitals allows us to assign the nature of their lowest excited singlet states: while for INP and KINP, it corresponds mainly to a π-π^* transition with charge transfer character, the other compounds exhibit a lowest excited state with $n\pi^*$ character, although the assignment is ambiguous for INS. The interactions of the molecules with the solvent are also discussed in the framework of a simple model based on dipole–dipole interactions.

DOI: 10.1039/b415876h

1. Introduction

UV radiation, especially UVB, represents one of the most important environmental factors affecting humans. It can give rise to mutations at the origin of skin cancer as well as premature skin aging. It is at these wavelengths that most cellular chromophores absorb, in particular DNA, since their absorption maxima match the action spectrum of UVB. Upon direct irradiation, adjacent pyrimidine bases, which are the main targets, lead to the formation of dimeric photoproducts, mainly cyclobutane thymine dimers at the origin of biological effects such as skin cancer and mutagenesis.[1] This damage can also be initiated under UVA irradiation by photosensitization involving a triplet-triplet energy transfer mechanism. It requires the triplet state of the photosensitizer to be higher in energy than that of thymine, which is the mononucleotide having the lowest triplet state. Only a few compounds such as acetone, acetophenone, benzophenone and indanone (IND) are efficient in this process, since they also have to exhibit a good intersystem crossing quantum yield.[2,3]

It has been recently reported that arylpropionic acid derivatives are also able to photosensitize the formation of these thymine dimers.[4,5] In the case of ketoprofen and fenofibric acid, their formation has been associated with the presence of the chromophore of benzophenone in their structure. For indoprofen (INP), whose photoreactivity occurs from its excited singlet state,[6] these photosensitizing properties towards DNA under UVA irradiation occur *via* its photochemical properties. Indeed, it has been shown recently that one of its photoproducts, 2-(4-acetylphenyl)isoindolin-1-one (KINP), is at the origin of the formation of thymine dimers.[7] Even though all the photoproducts of INP contain the same isoindolinone chromophore, only one of them, the acetyl derivative, also contains the acetophenone chromophore commonly described as a thymine dimer photosensitizer. Moreover, under the same irradiation conditions, IND with a high triplet state energy, photosensitizes the formation of thymine dimers whereas its nitrogenous derivative, 2-methylisoindoline does not (unpublished data).

In order to clarify the influence of the presence of the nitrogen atom and that of substitutions on the nature of the excited states of the chromophore of isoindolinone, spectroscopic and theoretical studies of 2-methylisoindolin-1-one (INS) have been performed and its photobiological properties towards DNA compared with those of indanone, indoprofen and 2-(4-acetylphenyl)isoindolin-1-one (Fig. 1).

Contemporary theoretical chemistry provides a wide variety of methods for the calculation of excited states of molecules. Among them, the time-dependent formulation of density functional theory (TDDFT)[8,9] provides vertical excitation energies to low-lying excited states with rather good accuracy,[10–15] despite some drawbacks, such as, in particular, the bad description of Rydberg states by GGA functionals.[16,17] This method requires less computational effort than multi-reference methods such as CASPT2,[18] and it allows several excited states to be studied. It thus becomes possible to perform routine theoretical calculations of UV spectra for molecules in the gas phase.[13]

However, it is well known that solute-solvent interactions modify the shape and intensities of observed spectra. According to Bayliss and McRae,[19,20] four cases can be considered for the interpretation of solvent shift effects on intramolecular

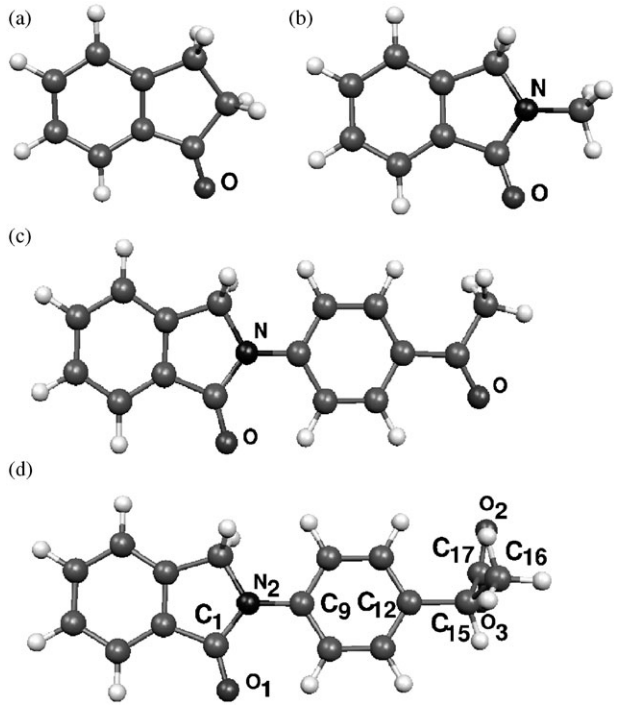

Fig. 1 Molecular structures of (a) indan-1-one (IND), (b) 2-methylisoindolin-1-one (INS), (c) 2-(4-acetylphenyl)isoindolin-1-one (KINP) and (d) 2-[4-(1-oxo-2-isoindolinyl)phenyl]propionic acid (INP) optimized at the DFT-B3LYP level of calculation.

electronic transitions: nonpolar solute in a nonpolar solvent, nonpolar solute in a polar solvent, dipolar solute in a nonpolar solvent and dipolar solute in a polar solvent. In the last of these cases, blue or red shifts are expected if the solute dipole moment decreases or increases in the excited state, respectively. From a theoretical point of view, the solvent can be regarded as a dielectric continuum and some methods are based on the classical reaction field model. Solvatochromic shifts will be theoretically investigated in the present work using the so-called polarizable continuum model (PCM), which is now a standard for the calculation of energies, structures and properties of molecules in solution.[21–23] Recently, a combined CASPT2/PCM and TDDFT/PCM study of the electronic spectrum of acrolein has shown that both methods give reasonably accurate results, in general agreement with experimental data.[24]

We will show that TDDFT calculations reproduce the electronic absorption spectra of indoprofen and of the three compounds that contain the isoindolinone chromophore with rather good accuracy, and that they provide valuable arguments for understanding the experimentally observed differences. Moreover, solvent effects are well-described by the combined TDDFT/continuum approach. They will be discussed in connection with the molecular orbitals (MOs) involved in the electronic excitations and an elementary model based on dipole–dipole interactions.

2. Methodology

2.1. Experimental

2-[4-(1-Oxo-2-isoindolinyl)phenyl]propionic acid, indan-1-one and 2-methylisoindolin-1-one were purchased from Sigma Chemical Co. (St. Quentin Fallavier, France). Absorption spectra in ethanol, diethyl ether and 5 mM phosphate buffered solutions (PBS) containing 10 mM NaCl at pH = 7.4 were measured by means of a HP 8452 A diode array spectrophotometer.

2.2. Theoretical calculations

All the calculations described below were performed with the GAUSSIAN 03 quantum chemistry package.[25] The geometries were optimized at the DFT level of theory. We have used the popular B3LYP hybrid functional in all cases. Geometry optimization was performed in the gas phase and in ethanol by means of the PCM model, using the 6-31G(d,p) basis set. In the PCM approach, the solute was embedded in a cavity formed by interlocking spheres, and the solvent reaction field was expressed in terms of a polarization charge density spread on the cavity surface. Pauling radii were used. The Franck–Condon vertical transitions were calculated for the optimal geometry in the ground state with the TD-B3LYP method and the same basis set, both in the gas phase and in ethanol. In the latter case, non-equilibrium solvation effects, which may occur during electronic excitation, were taken into account by splitting the solvation charge into two components: an fast electronic component of solvent polarization in equilibrium with the solute electronic density and a slow component, delayed when the solute undergoes a sudden transformation.[26,27] We calculated wavelengths, corresponding to vertical transitions from S_0 to a singlet excited state S_i, and oscillator strengths of each $S_0 \rightarrow S_i$ transition, in order to compare with experimental intensities and to analyze the nature of the main excited states involved in intense bands. It should thus be recalled that the TDDFT wavefunction, Ψ_I for the Ith excited state, has the form:[16]

$$\Psi_I = \sum_{i\in\mathrm{occ}} \sum_{j\in\mathrm{virt}} C_{ij}^I \Phi_{i\rightarrow j}$$

where $\phi_{i\rightarrow j}$ is the determinant representing an excitation from the occupied MO φ_i towards the virtual MO ψ_j and C_{ij}^I is the weight of that determinant in the wavefunction Ψ_I. Thus, the analysis of the nature of the states was supported by the values of the C_{ij}^I coefficients in the TDB3LYP wavefunction and by the shapes of the B3LYP MOs. Following several authors (see, for example, Baerends and co-workers[28] and Stowasser and Hoffmann[29]), it was assumed that the DFT MOs were suitable for a good description of the electronic structure of molecules, as Hartree–Fock or extended Hückel MOs. Since vibrational motion of atoms and solute-solvent dynamical interactions were not taken into account, peaks were obtained instead of bands. For the purpose of comparison with the experimental spectra, the peaks were convoluted with Gaussian-type functions, as is usually done. The width of the Gaussian functions was chosen in order to reproduce the experimental bandwidth qualitatively. Fifteen singlet excited states were computed for IND and INS in order to cover the range of wavelengths above 170 nm. Since the density of states increases in that range for the largest systems, 30 singlet excited states were calculated for INP and KINP.

As shown hereafter, the largest discrepancy between theory and experimental results was observed for INS. For this reason, we have checked that there was no significant basis set or functional effect on the position of the lowest excited states and, consequently, on the shape of the theoretical electronic absorption spectrum. This is shown in Fig. 2 where the ground state molecular structures of INS were optimized with the 6-311G(d,p) basis set whereas vertical excitation energies were computed using the 6-311++G(d,p) basis set. It can be seen that the spectra obtained with the 6-31G(d,p) and 6-311++G(d,p) basis sets are rather similar, with only slight red and blue shifts of the π-π* and n-π* transitions, respectively. High excited states, which are stabilized with the largest basis set and appear near 200 nm with respect to S_0, do not lead to a significantly different spectrum. Moreover, no significant differences are observed in the relative intensities. As expected, TDDFT excitation energies and oscillator strengths depend only weakly on basis sets. We have also

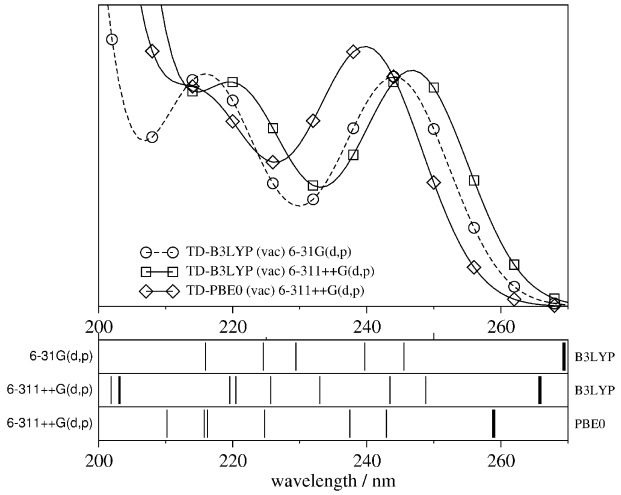

Fig. 2 Evaluation of functional and basis set effects on the electronic absorption spectrum of INS. The positions of all the transitions to the low-lying excited states are shown below the spectra (the thick bars correspond to the n-π* transition).

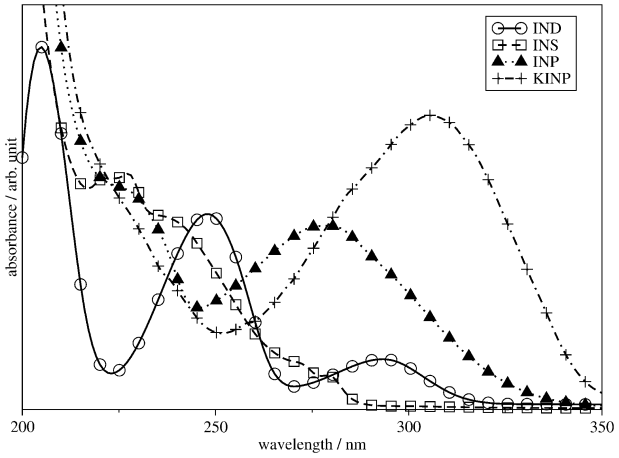

Fig. 3 Experimental absorption spectra of: (○) IND, (□) INS, (▲) INP and (+) KINP in 5 mM phosphate buffered solution (PBS) containing 10 mM NaCl at pH = 7.4

investigated whether the PBE0 functional, known to sometimes provide spectroscopic data in better agreement with experimental data than B3LYP,[30] could yield better results or not. It can be seen in Fig. 2 that the B3LYP and PBE0 results are similar. As a consequence, we assumed here that B3LYP calculations performed with the 6-31G(d,p) basis set were accurate enough to provide explanations of the differences observed in the absorption spectra and solvent shift effects from the four compounds considered in this work.

3. Experimental results

The absorption spectrum of INS is characterized by three transitions of different intensities (Fig. 3). Two of the three bands appear split in two, maybe due to a vibrational pattern; their absorption maxima are at 222 and 228 nm ($\varepsilon \sim 7800$ M^{-1} cm^{-1}) for the first one and 272 and 280 nm ($\varepsilon = 1360$ M^{-1} cm^{-1}) for the second. The third transition is characterized by a broad band at ~240 nm that partially overlaps the neighbouring bands, preventing the determination of its spectral characteristics. Nonetheless, the nature of the two other transitions has been identified. The band with λ_{max} at 280 nm undergoes a slight bathochromic shift with increasing solvent polarity (λ_{max} = 278 nm in ethanol and 280 nm in PBS). This shift, together with the relatively high absorption coefficient of the band, indicates a transition of π-π* nature. Although its absorption maximum is unchanged whatever the solvent, the band at 228 nm is also attributed to a π-π* transition, due to the high value of its molar absorption coefficient. Finally, no n-π* band was found.

To investigate the influence of the nitrogen atom on the spectroscopic properties of INS, we compared the absorption spectra of INS and IND. Though the absorption spectra of these two compounds show some similarities, their general pattern is different. Indeed, if INS, as IND, exhibits two absorption bands of π-π* nature,[31] the presence of a very broad band in the 240 nm region alters considerably the general pattern of the absorption spectrum of INS. Moreover, INS does not seem to possess an excitation of n-π* nature, which would be expected to lie above 300 nm, as for IND.

In order to study the effect of N-substitution on the isoindolinone chromophore, we compared the spectroscopic properties of INS and INP in PBS. The first π-π* bands (λ_{max} = 228 nm) of the two compounds are very similar, since they show the same absorption maximum, with a moderate blue shift and very similar molar absorption coefficients. The second π-π* band of INS also has the same absorption maximum as that of INP, but with a lower molar absorption coefficient (ε = 1360 for INS and 13 500 M^{-1} cm^{-1} for INP).[6] Although the solvent polarity has little effect on this electronic band, it does not affect the ground state of these molecules in the same way, since for INS a moderate red shift is observed instead of a moderate blue shift in the case of INP.

The role of the acetophenone chromophore on the properties of KINP was also investigated. Its absorption spectrum recorded under the same conditions also contains two π-π* bands, the first one being very similar to that of INS and INP (λ_{max} = 224 nm, no shift), while the second appears shifted to higher wavelength and shows a stronger absorbance than the corresponding band of INP (in ethanol, λ_{max} = 306 nm, ε = 31 000 M^{-1} cm^{-1}).

4. Theoretical results and discussion

4.1. Ground-state geometries

IND and INS possess similar structures: the average carbon-carbon distance in the six-membered rings is 1.398 and 1.396 Å, respectively, and the C=O distances are 1.217 and 1.223 Å, respectively. In KINP, the acetophenone and isoindoline moieties are in the same plane due to delocalization of the π electrons. Two isomers were found for INP, differing in the rotation of the propionic acid moiety with respect to the phenyl ring, and separated by only 0.2 kcal mol^{-1}. INP adopts a planar conformation, except for the propionic acid moiety, which is twisted out of the plane of the phenyl ring in both isomers [Fig. 1(d)]. The second isomer's structure is very close to a previously reported X-ray structure.[32] A set of selected distances and angles is reported in Table 1. While the distances and angles of the DFT-calculated structures are very close to the experimental data, the dihedral angles, which characterize the rotation of the acid group, differ somewhat from the experimental values. This can be rationalized by the observed formation of a centrosymmetric dimer through intermolecular hydrogen bonds between two carboxylic acid groups in the crystal phase, which leads to a local distortion of the propionic acid moiety relative to the plane.

4.2. Gas phase electronic absorption spectra

IND. The theoretical and experimental UV spectra of IND are given in Fig. 4. TDDFT calculations show that only four singlet excited states account for the transitions in the 200–350 nm range. The S_1 state absorbs very weakly, with an oscillator

Table 1 Selected geometric parameters of INP (distances in Å and angles in °).

		Theoretical	
	Experimental[32]	Lowest energy isomer	X-Ray[32] isomer
C_1–O_1	1.236	1.222	1.222
C_{17}–O_3	1.262	1.352	1.354
C_{17}–O_2	1.219	1.213	1.213
C_9–N_2	1.410	1.412	1.412
C_{12}–C_{15}	1.538	1.527	1.527
C_1–N_2–C_9	127.5	126.8	126.8
C_1–N_2–C_8	111.2	111.9	111.9
C_{13}–C_{12}–C_{15}	124.5	120.8	121.4
C_1–N_2–C_9–C_{10}	178.6	180.0	179.5
C_{11}–C_{12}–C_{15}–C_{17}	154.0	−53.4	125.4
C_{13}–C_{12}–C_{15}–C_{16}	97.3	−109.1	67.1
C_{12}–C_{15}–C_{17}–O_3	−80.6	−91.4	−87.2
C_{16}–C_{15}–C_{17}–O_2	−26.4	−36.7	−32.7

strength $f_1 = 0.0001$. This corresponds mainly to an excitation from MO φ_1 to MO ψ_1 (Fig. 5), that is to say, from the oxygen lone pair orbital n to a π* MO delocalized over the phenyl ring and the C=O chromophore. The three other states have ππ* character: each of them is mainly described by a single excitation from MO φ_2, φ_3 and φ_4 to the ψ_1 MO (see assignment in Fig. 4). S_2 and S_4 absorb significantly ($f_2 = 0.0320$ and $f_4 = 0.1774$), whereas the oscillator strength of the $S_0 \rightarrow S_3$ transition is very weak. The $S_0 \rightarrow S_2$ and $S_0 \rightarrow S_4$ transitions are well-separated, since they lie at 259 nm and 231 nm, respectively. As a consequence, each of them describes one of the two experimentally observed π-π* bands. The π-π* bands are blue-shifted by 7 and 29 nm with respect to the spectrum obtained in diethyl ether, whereas the n-π* transition is red-shifted by 20 nm. Nevertheless, considering the relative intensities and the positions of the π-π* and n-π* bands, the TDDFT calculations are overall in good agreement with the experiment.

INS. Direct comparison of the theoretical and experimental spectra, given in Fig. 6, indicates that the data do not agree as well as for IND, so that the assignment is ambiguous. The lowest singlet excited state S_1 is calculated to give a transition at $\lambda = 269$ nm, which corresponds to an excitation from φ_2 to ψ_1 (Fig. 5), that is, it has n-π* character. As expected for such transitions, its oscillator strength is very weak ($f_1 = 0.0001$). Although the experimental band with $\lambda_{max} = 280$ nm, which

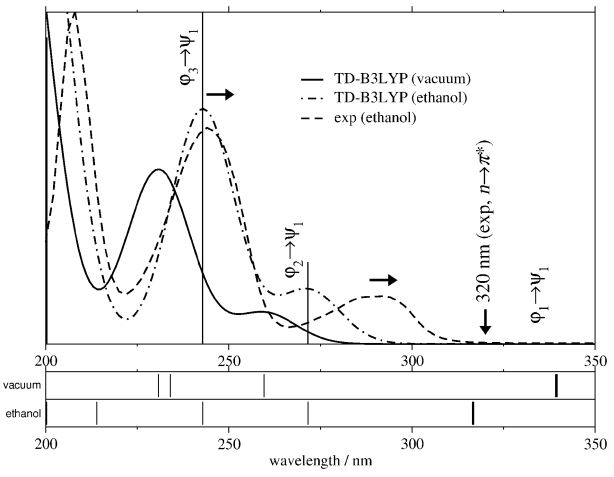

Fig. 4 Theoretical and experimental absorption spectra of IND. The vertical lines show the positions and intensities of the vertical transitions used for the convolution of the theoretical spectrum in ethanol. The theoretical wavelengths of the transitions are given below; the thick bars correspond to the n-π* transitions. The horizontal arrows indicate the experimental solvatochromic shift.

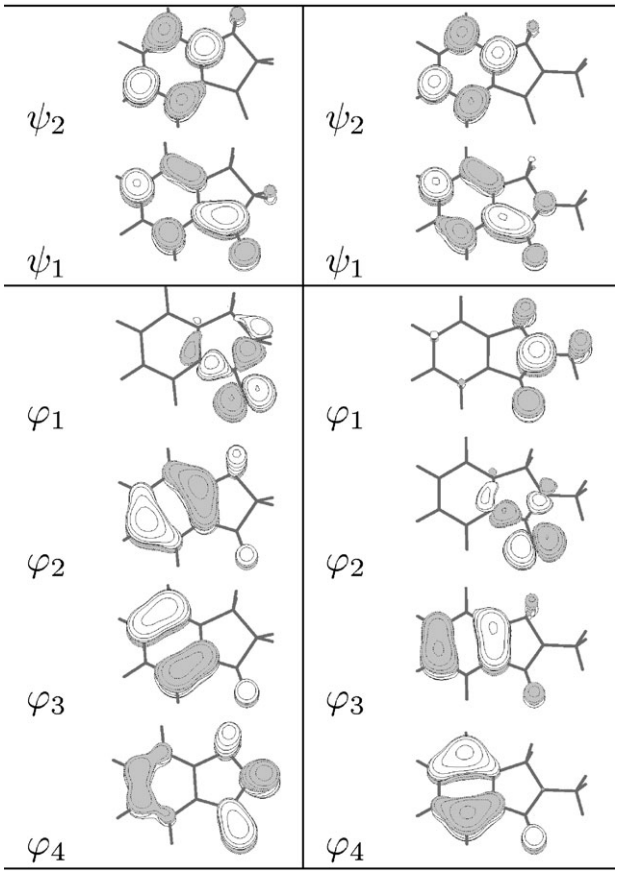

Fig. 5 Highest occupied MOs (φ_i) and lowest unoccupied MOs (ψ_i) of IND (left) and INS (right).

has the intensity and the solvatochromic property of a π-π* band, should not be assigned to S_1, it will be shown in the discussion of solvent effects that, among other possibilities, this situation may still be considered. Numerous ππ* states lie above S_1 and a given band cannot be assigned to a single $S_0 \rightarrow S_i$ transition. Two relatively intense transitions occur at 246 and 240 nm ($f_2 = 0.0724$ and $f_3 = 0.0250$). Regarding S_2, the excitation is generated from the HOMO (φ_1), which is mainly concentrated on the orthogonal n_π orbital of the nitrogen atom, towards the LUMO (ψ_1). These two states explain the intermediate band experimentally observed at approximately 240 nm. Finally, the position of the $S_0 \rightarrow S_6$ transition ($\lambda = 216$

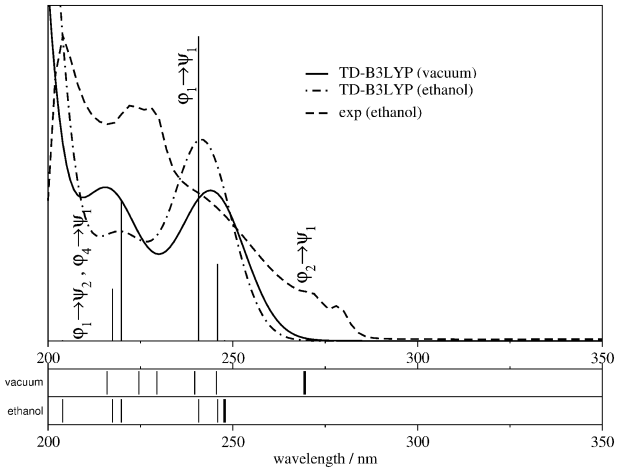

Fig. 6 Theoretical and experimental absorption spectra of INS. The vertical lines show the positions and intensities of the vertical transitions used for the convolution of the theoretical spectrum in ethanol. The theoretical wavelengths of the transitions are given below; the thick bars correspond to the n-π* transitions.

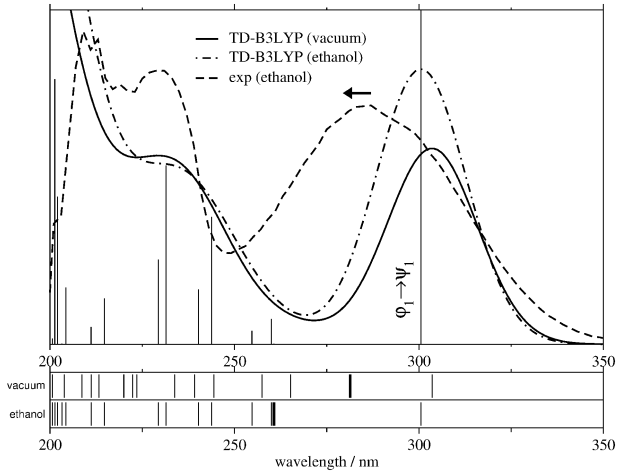

Fig. 7 Theoretical and experimental absorption spectra of INP. The vertical lines show the positions and intensities of the vertical transitions used for the convolution of the theoretical spectrum in ethanol. The theoretical wavelengths of the transitions are given below; the thick bars correspond to the n-π* transitions. The horizontal arrow indicates the experimental solvatochromic shift.

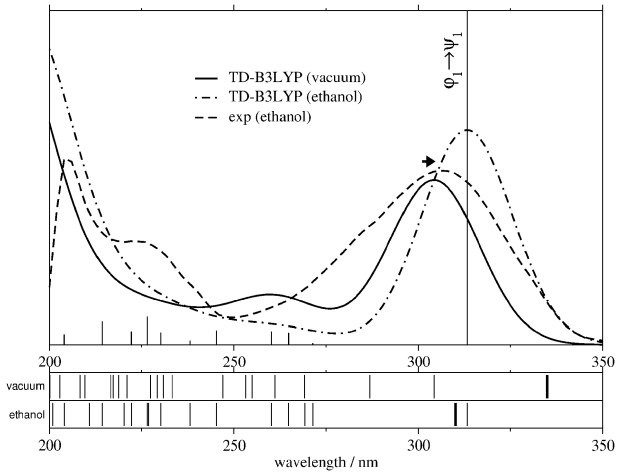

Fig. 9 Theoretical and experimental absorption spectra of KINP. The vertical lines show the positions and intensities of the vertical transitions used for the convolution of the theoretical spectrum in ethanol. The theoretical wavelengths of the transitions are given below; the thick bars correspond to the n-π* transitions. The horizontal arrow indicates the experimental solvatochromic shift.

nm), which also has a large oscillator strength (f_6 = 0.0929), agrees well with the lowest wavelength band (λ_{max} = 228 nm in diethyl ether). It should be noted that this oscillator strength is lower than f_4 for IND, in agreement with the decrease of ε_{max} (13 000 and ~7800). In summary, except for the fact that the lowest band cannot be unambiguously assigned to S_1, it can be stated that there is a fair overall agreement and that the observed different absorption features of INS and IND are well reproduced by TDDFT calculations.

INP. The calculated and theoretical spectra of INP are very similar. The most striking feature is the appearance of an intense band at λ_{max} = 304 nm (f_1 = 0.3653), close to the experimental band observed at λ_{max} = 284 nm (Fig. 7). This π-π* band is described by a transition from an MO localized on the phenylpropionic acid group towards an MO localized on the isoindolinone chromophore moiety (φ_1 and ψ_1 in Fig. 8, respectively). This transition leads to a large rearrangement of the electronic density of the whole molecule and it can be viewed as a charge transfer (CT). The overlap between φ_1 and ψ_1 is weak; the large oscillator strength cannot be explained by Franck–Condon factors but rather by this CT character, which induces a large transition dipole moment. From our calculations, the n-π* transition lies at 282 nm, that is, above the π-π* one. Consequently, it is hidden by this intense π-π* band and cannot be observed experimentally. INP is a large conjugated system and the number of π-π* transitions lying in a narrow range increases. As a matter of fact, the calculations show that 13 π-π* transitions lie in the range 200–265 nm. The band observed at 228 nm can be mainly described by three π-π* transitions with smaller oscillator strengths than the $S_0 \rightarrow S_1$ transition (f_6 = 0.1421, f_7 = 0.1020, f_8 = 0.1144). However, they are very close (λ_6 = 239, λ_7 = 234, λ_8 = 224 nm) and their convolution leads to a single π-π* band, equally intense as the low-energy band, in agreement with the experiment.

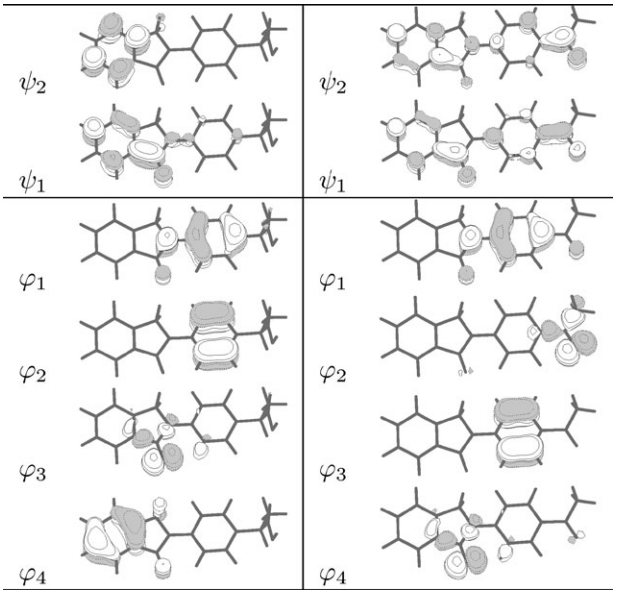

Fig. 8 Highest occupied MOs (φ_i) and lowest unoccupied MOs (ψ_i) of INP (left) and KINP (right).

KINP. INP and its photoproduct, KINP, exhibit similar UV absorption spectra, with two intense bands at λ_{max} = 306 nm and λ_{max} = 224 nm in ethanol for the latter (Fig. 9). The calculated transition to the second singlet state occurs at 304 nm with a large oscillator strength (f_2 = 0.5695), and may be assigned to the lowest energy experimental band. Its nature is analogous to the intense CT band of INP: a transition from φ_1, mainly localized on the acetylphenyl chromophore, towards ψ_1, the first π* MO (Fig. 8). However, while ψ_1 is mainly localized on the isoindolinone moiety in the case of INP, it exhibits a much more pronounced delocalization in KINP, that is to say, with less CT character. Although the density of π-π* transitions between 200 and 300 nm is quite large, the lowest band is due to this S_0 state → CT state transition. It is interesting to note that this band exhibits a stronger absorbance than for INP (ε = 31 000 and 13 500 M^{-1} cm^{-1} for KINP and INP, respectively, *i.e.*, a ratio of 2.3 : 1). This can be related to the respective oscillator strengths of these two compounds (f_2 = 0.5695 and f_1 = 0.3653, respectively, *i.e.*, a ratio of 1.6 : 1). Although the agreement between the relative intensities of the lowest band of INP and KINP is rather good, a slight discrepancy can be observed for the high-energy band. As a matter of fact, the oscillator strengths of the π-π* transitions of KINP in the range 200–250 nm are lower than those of INP. Although this is inconsistent with the experiment, we assume that the oscillator strengths are slightly underestimated with respect to the absorption of the states above 200 nm, and their convolution does not lead to the band observed at λ_{max} = 228 nm. Finally, the n-π* transition lies

Table 2 λ_{max} of the electronic absorption spectra of IND, INS, INP, and KINP under different conditions: experimental and theoretical data.

	Experimental λ_{max}/nm			Theoretical λ_{max}/nm			$\Delta\lambda^b$/nm	
	Diethyl ether (DEE)	Phosphate buffer (PBS)[a]	Δ_{exptal}	Vacuum	Ethanol (EtOH)	Δ_{theory}	$\lambda_{DEE} - \lambda_{vac}$	$\lambda_{PBS} - \lambda_{EtOH}$
IND	238	248 (13 000)	+10	231	243	+12	−7	−5
	284, 292	294 (3000)	+10	259	271	+12	−29	−23
INS	228	228 (~7800)	0	215	~220	+5	−13	−8
	~240	~240	~0	244	241	−3	~−4	~0
	276	280 (1360)	+4	269	?	?	−8	?
INP	228	228 (~13 500)	0	229	~229	0	+1	+1
	284	280 (13 500)	−4	304	301	−3	+18	+21
KINP	306	308 (~31 000)	+2	304	313	+9	−2	+5

[a] ε_{max} (in M^{-1} cm^{-1}) is given in parentheses. [b] Δ_λ is the difference between experimental and theoretical wavelength values in diethyl ether and vacuum or phosphate buffer and ethanol.

at 335 nm and is probably hidden in the wing of the intense $\varphi_1 \rightarrow \psi_1$ band.

Discussion. The experimental values of λ_{max} in diethyl ether, a weakly polar solvent, and the theoretical values of λ_{max} in vacuum are summarized in Table 2. $\Delta\lambda$ is calculated as λ_{max}(theory) − λ_{max}(exptal) and indicates the difference between theory and experiment. With the exception of INS, for which the attribution of the bands is less clearcut than for the other compounds, the agreement is good. All theoretical and experimental spectra look similar. Theoretical transition energies are in general overestimated, and theoretical spectra are thus systematically blue-shifted with respect to experimental observations, except for the low-energy band of INP. This is not surprising: the corresponding excited state exhibits the largest CT character and it is known that TDDFT energies for CT states are underestimated.[17,33] $\Delta\lambda$ is less than 30 nm in all cases. Again, INS deserves a special discussion, which will be given in the section devoted to solvent effects. As a matter of fact, while the intermediate band very likely corresponds to the excitation from the HOMO (φ_1) to the LUMO (ψ_1), it is not clear that the long-wavelength band has an n-π* character with an anomalous intensity. From a more methodological point of view, it is well-known that in the current implementation of TDDFT, long-range CT excited states are sometimes badly described, due to an incorrect $1/r$ asymptotic behaviour of the exchange–correlation functionals (r being the electron-to-nucleus distance).[33] Thus, TDDFT underestimates the excitation energies of such states, often involved in extended π systems.[34] In the present case, the CT states of INP and KINP agree with the experimental features. Thus, it seems that, according to the experimental data, this important weakness of the method is not observed here.

Regarding the intense CT band observed for INP and KINP only, this can be understood by means of elementary MO theory. Fig. 10 displays a simple MO interaction diagram between the π and π* frontier orbitals of the isoindolinone and phenyl (Ph) moieties, obtained by simple Hückel calculations. This energy-level diagram permits a ready visualization of the large bathochromic shift of the transition, which corresponds to the excitation from φ_1 to ψ_1 in INS. The theoretical wavelengths in vacuum, corresponding to the $\varphi_1 \rightarrow \psi_1$ transition for INS, INP and KINP, are 244, 304 and 304 nm, respectively. According to our assignments of the experimental bands, the λ_{max} values for these three compounds are 240, 286 and 306 nm in diethyl ether. In INP and KINP, the φ_1 and ψ_1 MO mix with the π_1 and π_1* MO of Ph, respectively. This results in a stabilization of ψ_1 and a destabilization of φ_1 and, consequently, a decrease in the energy difference between the frontier orbitals. Moreover, this φ_1-ψ_1 transition acquires some CT character from the phenyl ring to the isoindolinone chromophore, and this excitation from the ground state gains in intensity. Finally, the CT nature depends on the strength of the interaction between the LUMO of INS and Ph. In the case of KINP, the π* MO of CMeO interacts strongly with the π_1* of Ph, resulting in a stabilization of the LUMO, a better mixing between π_1*(Ph) and π_1*(INS), and a reduction of the CT character.

4.3. Solvent effects

Results. The geometries of the four compounds have been re-optimized in ethanol, using the PCM model, and the combined TDDFT/PCM approach has been used to evaluate their solvatochromic behaviour. In principle better results could be obtained by representing the first solvation shell with explicit solvent molecules and using a continuum for the bulk,[35] but this approach is not easy to handle, and the continuum model has previously proven its ability to provide results in good agreement with experiments. The positions of the transitions as well as their relative intensities and the convolution of the peaks are superimposed on Figs. 4, 6, 7 and 9. The expected solvent effects on the relative positions of the bands are observed: the weak n-π* bands are systematically blue-shifted, whereas the π-π* bands are in general red-shifted. The experimental values of λ_{max} in solvents of different polarities and the theoretical values of λ_{max} in vacuum and ethanol are summarized in Table 2. A comparison of the variation in the positions of the bands with increasing polarity of the solvent is also given (Δ_{exptal} and Δ_{theory}). The experimental and theoretical solvato-

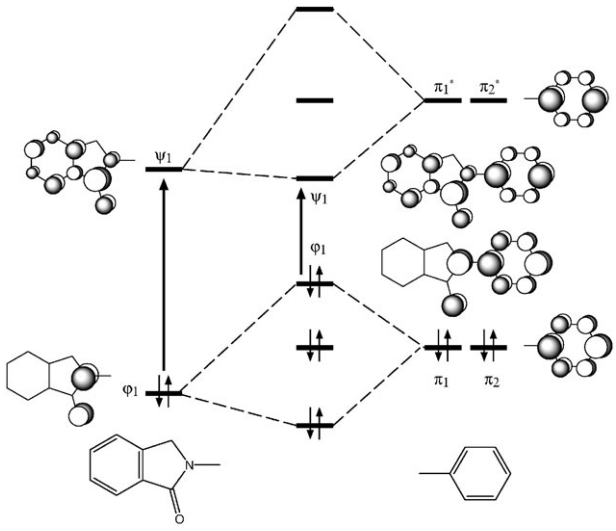

Fig. 10 MO interaction diagram between the frontier orbitals of isoindolinone and phenyl groups, where φ_i and ψ_i are the highest occupied and lowest unoccupied MOs, respectively.

chromic shifts are similar. The large positive solvatochromism of the two bands of IND are well-reproduced (+10 nm *vs.* +12 nm). The red-shift of the CT band of KINP is also observed, although it is slightly overestimated. In contrast, the CT band of INP is blue-shifted, in both theory and experiment.

An unambiguous assignment of the experimental bands of INS is difficult; thus, we shall only formulate suggestions. From the calculations done in the gas phase, the transition to the lowest excited state has nπ* character and, hence, the corresponding $S_0 \rightarrow S_1$ transition exhibits a very small oscillator strength. According to TDDFT and PCM, this transition is, as expected, significantly blue-shifted. Unfortunately, this is in disagreement with the experimental observation and no excited state in ethanol absorbs in a domain around the lowest energy band. Although perfect agreement cannot be expected between theory and experiment, the difference between λ_{max} and the absorption wavelength for the first excited states are unreasonably large. We have thus performed other calculations in which 25 explicit water molecules were introduced in the first solvation shell of the solute and their positions relative to INS were optimized. The presence of water molecules leads to a mixing of the $\varphi_2\psi_1$ and $\varphi_1\psi_1$ configurations in S_1. The lowest excited state is now no longer a pure nπ* state, but develops some $n_\pi\pi^*$ character (φ_1 can roughly be regarded as the nitrogen lone pair participating in the π system and remaining essentially localized on N). While the wavelength is not significantly changed with respect to gas phase calculations, the oscillator strength is enhanced by an order of magnitude. The S_1 state absorbs more strongly due to the presence of water molecules. Analogous results are obtained if the number of water molecules is decreased or increased within moderate limits. Of course, it would be necessary to saturate the second and third solvation shells, in particular in order to describe packing effects. However, this result leads to an interesting suggestion: the lowest state may not have a pure nπ* character, due to the nitrogen atom. The mixing of nπ* and ππ* characters could explain the observed solvatochromism, dominated by the ππ* component, and the vibrational structure of the band, similar to an nπ* state. On the other hand, one cannot rule out the possibility that the energy of the S_2 state is significantly overestimated, similarly to the S_2 state of IND, whose transition is blue-shifted by 23 nm with respect to the experimental value. Finally, we have also performed TDDFT calculations using the Casida–Salahub asymptotic correction [16] with the Zhan, Nichols and Dixon empirical formulation[36] by means of the NWChem package.[37] No dramatic changes of the vertical transition energies and oscillator strengths are observed, compared to standard TDB3LYP calculations.

Dipolar solute in a polar solvent: a simple vectorial model for solvatochromism. Bathochromic and hypsochromic shifts are suitably taken into account if the solvent is described as a structureless fluid. In particular, the TDB3LYP/PCM approach accounts well for the different behaviour of the CT band of INP and KINP although, according to the analysis of the TDDFT wavefunction, the CT state seems similar in both cases. In the following, we provide arguments for understanding the differences between INP and KINP in terms of the variation of both the absolute magnitude and the angle of the dipole moment in the ground state (μ_0) and in the excited state (μ_i). It should be recalled that equations for the dipole–dipole interactions can be derived, leading to the possibility to determine experimentally the variation of the dipole moment between the ground state and the excited state by means of absorption and fluorescence spectra. However, the expression of the Stokes shift ($\bar{\nu}_{abs} - \bar{\nu}_{fluo}$) depends only on the absolute magnitude of the dipole moment ($\mu_0 - \mu_i$) and not on the angle between the dipoles.[20] Regarding absorption spectra, various models based on a continuous description of the solvent have been proposed. In usual formulations, such as the Bayliss–McRae model of solvatochromism,[20] the energy of an absorption band in the gas phase and in solution depends on the refractive index n, on the bulk static relative permittivity ε and on the angle ϕ between the ground and excited state dipoles. We propose here a crude model, intended to provide a qualitative picture of dipolar solute-polar solvent interactions. It is based on the variation of the dipole moment value and orientation in an excited state with respect to the ground state, in the framework of Franck–Condon excitations, considering explicit solute and solvent molecules. In an idealized vision of the interactions, the dipole moment of the solvent molecules (μ_s) in the first solvation shell are oriented according to the orientation of μ_0 [Fig. 11(a)]. The classical interaction potential between two dipoles μ_1 and μ_2 is given by:

$$V_{12} = \frac{\mu_1 \times \mu_2}{r^3} - 3\frac{(\mu_1 \times r)(\mu_2 \times r)}{r^5} \qquad (1)$$

where r is the vector between the two dipoles. Since V_{12} decreases rapidly as r increases, we propose a rough approximation, consisting in the reduction of the whole solvent–solute system to two polar solvent molecules perfectly aligned along the ground state dipole moment of the solute, that is, the solvent molecules considered here are those the closest to the solute [Fig. 11(b)]. The variation of the interaction potential between an excited state S_i and the ground state S_0 becomes:

$$\Delta V_{i0} = V_{is} - V_{0s} = K_{||}(1 - c\cos\phi) \qquad (2)$$

with $K_{||} = 4\mu_0\mu_s/r_{||}^3$ and $c = \mu_i/\mu_0$. Thus, ΔV depends on the variation of the angle ϕ between μ_0 and μ_i and the factor of proportionality (c) between μ_0 and μ_i.

The variation of ΔV_{i0} as a function of ϕ for different values of c is given in Fig. 12. At both limits, the model is in agreement with the behaviour expected intuitively: if the excitation leads to a dipole flip ($\phi = 180°$), the excited state

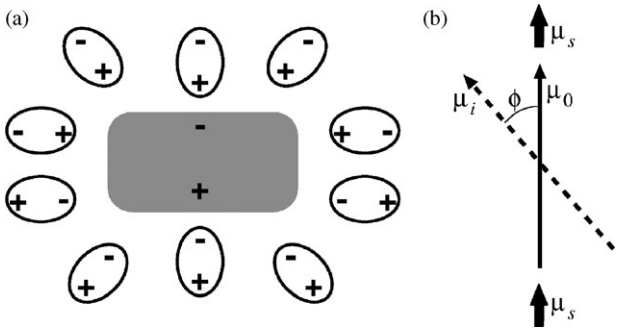

Fig. 11 (a) Polar solvent cage around a dipolar solute. (b) Model of dipole–dipole interaction between a polar solute and two polar solvent molecules.

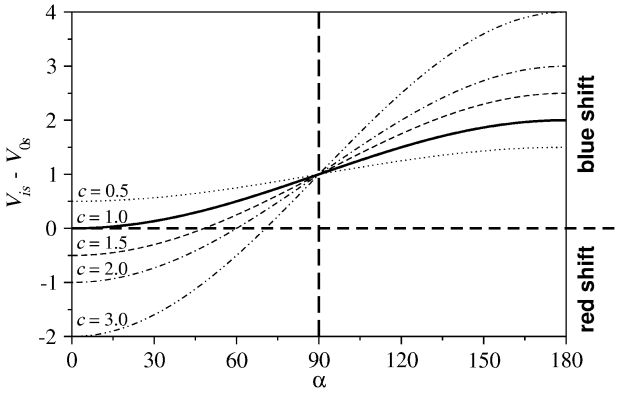

Fig. 12 Variation of the dipole–dipole interaction potential between an excited state S_i and a ground state S_0, according to the model given in Fig. 11(b).

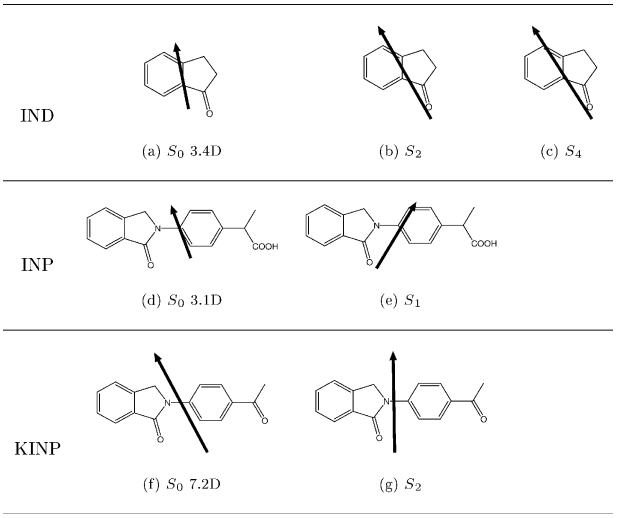

Fig. 13 B3LYP dipole moments of IND, INP and KINP in S_0 and qualitative dipole moments in selected excited states. The dipole moment of INS in its ground state is 3.9 D.

is destabilized and this produces a hypsochromic shift, whatever the magnitude of μ_i; if the orientation of the dipole is not altered in S_i ($\phi = 0°$), a red shift is observed if $\mu_i > \mu_0$, while a blue shift is obtained if $\mu_i < \mu_0$. Of course, the model should be refined by adding other solvent dipoles and by taking into account dipole-induced-dipole terms and dynamic effects; such work is in progress. Still, the present results provide a pedagogic insight into the solvatochromic domains intermediate between $\phi = 0°$ and $\phi = 180°$. For example, for $\phi = 45°$, bathochromic shifts will be observed if $\mu_i > 1.5\ \mu_0$, while blue shifts are expected when $\mu_i < 1.5\ \mu_0$. The explanation for the different solvatochromism of INP and KINP may lie in this aspect.

Unfortunately, calculation of dipole moments for TDDFT excited states is not trivial, since it requires finite field calculations,[38] which are beyond the scope of this first paper. However, the analysis of the nature of the excitations that lead to a given excited state S_i allows us to deduce qualitatively the approximate re-orientation of the dipole moment in that state. Fig. 13 shows the dipole moment calculated in the ground state, as well as the qualitative dipole moments in selected excited states deduced by the analysis of the MOs involved in the excitation. When comparing INP and KINP, their MOs reveal a better overlap between φ_1 and ψ_1 in KINP, that is, a less pronounced CT character. We infer that the angle between μ_0 and μ_1 in INP is much larger than the angle between μ_0 and μ_2 in KINP. Considering the arguments previously given within the framework of our model, this should result in a decrease of λ_{max} for the CT band of INP. As far as IND is concerned, the excitation should only involve a significant increase of the dipole moment without variation of its orientation, thus resulting in a positive solvatochromism. Finally, since the bands of INS cannot be assigned to a single excited state, their solvatochromic property remains unclear.

5. Conclusion

We have explored the behaviour of the PCM model coupled with TDDFT for the evaluation of solvatochromic shifts in electronic absorption spectra of compounds involved in DNA damage. The results are in good agreement with the experimental data and provide insight into the low-lying excited states of these molecules and the solvatochromic shifts of the UV bands.

We have shown, in particular, that the influence of the n_π lone pair of the nitrogen atom allows a delocalization of the π electrons between the INS moiety and a conjugated fragment bound to N. Consequently, a low-energy state with a substantial CT character appears in molecules such as INP and KINP. Additional calculations on 2-[4-(2,3-dihydro-1-oxo-1*H*-inden-2-yl)phenyl]propanoic acid and 2-(4-acetylphenyl)-2,3-dihydroinden-1-one, not described in this paper, have confirmed that the presence of the IND chromophore in larger systems does not lead to a CT state since the nonplanarity of the linking carbon does not allow good conjugation between the IND moiety and the substituted phenyl fragment.

The only major discrepancy concerns INS, which we have studied in greater detail: explicit treatment of the solvent and asymptotically corrected functionals. According to TDDFT, an explicit treatment of the solvent may induce a coupling between the $n\pi^*$ and the $n_\pi\pi^*$ configurations, where n and n_π are the lone pairs of the oxygen and nitrogen atoms, respectively. However, one cannot rule out that this could be a problem within TDDFT, which could overestimate the energy of some states of INS, although the known failures of this method usually concern Rydberg states and intra- or intermolecular CT states of large π systems.[17,33,34,39]

In summary, this combined TDDFT/PCM approach appears very powerful for exploring the properties of the excited states of indanone and isoindolinone compounds.

Acknowledgements

F.G. and R.P. thank the CALcul en MIdi-Pyrénées (CALMIP) and the Centre Informatique National de l'Enseignement Supérieur (CINES) for allocations of computational resources. The authors gratefully acknowledge Prof. C. Marsden for careful reading of the manuscript.

References

1 A. Gentil, F. Le Page and A. Sarasin, *Biol. Chem.*, 1997, **378**, 1287–1292.
2 I. G. Gut, P. D. Wood and R. W. Redmond, *J. Am. Chem. Soc.*, 1996, **118**, 2366–2373.
3 P. D. Wood and R. W. Redmond, *J. Am. Chem. Soc.*, 1996, **118**, 4256–4263.
4 V. Lhiaubet, N. Paillous and N. Chouini-Lalanne, *Photochem. Photobiol.*, 2001, **74**, 670–678.
5 J. Trzcionka, V. Lhiaubet-Vallet and N. Chouini-Lalanne, *Photochem. Photobio. Sci.*, 2004, 226–330.
6 V. Lhiaubet-Vallet, J. Trzcionka, S. Encinas, M. A. Miranda and N. Chouini-Lalanne, *Photochem. Photobiol.*, 2003, **77**, 487–491.
7 V. Lhiaubet-Vallet, J. Trzcionka, S. Encinas, M. A. Miranda and N. Chouinia-Lalanne, *J. Phys. Chem. B.*, 2004, **108**, 14148–14153.
8 K. Burke and E. K. U. Gross, in *Density Functional: Theory and Applications*, ed. D. Joubert, Springer, Berlin, 1998, pp. 117–146.
9 C. Jamorski, M. E. Casida and D. R. Salahub, *J. Chem. Phys*, 1996, **104**, 5134–5147.
10 R. Bauernschmitt, R. Ahlrichs, F. H. Hennrich and M. M. Kappes, *J. Am. Chem. Soc.*, 1998, **120**, 5052–5059.
11 S. J. A. Ginsbergen, A. Rosa, G. Ricciardi and E. J. Baerends, *J. Chem. Phys*, 1999, **111**, 2499–2506.
12 C. Adamo and V. Barone, *Theor. Chem. Acc.*, 2000, **105**, 169–172.
13 V. Lhiaubet, F. Gutierrez, F. Penaud-Berruyer, E. Amouyal, J.-P. Daudey, R. Poteau, N. Chouini-Lalanne and N. Paillous, *New. J. Chem.*, 2000, **24**, 403–410.
14 I. Ciofini, C. A. Daul and C. Adamo, *J. Phys. Chem. A*, 2003, **107**, 11182–11190.
15 F. Aquilante, V. Barone and B. O. Roos, *J. Chem. Phys*, 2003, **119**, 12323–12334.
16 M. E. Casida, C. Jamorski, K. C. Casida and D. R. Salahub, *J. Chem. Phys*, 1998, **108**, 4439–4449.
17 D. J. Tozer, R. G. Amos, N. C. Handy, B. O. Roos and L. Serrano-Andrés, *Mol. Phys.*, 1999, **97**, 859–868.
18 B. O. Roos, *Acc. Chem. Res.*, 1999, **32**, 137–144.
19 N. S. Bayliss and E. G. McRae, *J. Phys. Chem.*, 1954, **58**, 1002–1006.
20 C. Reichardt, *Solvents and Solvent Effects in Organic Chemistry*, VCH, Weinheim, 1988.
21 S. Miertus, E. Scrocco and J. Tomasi, *Chem. Phys.*, 1981, **55** 117–129.
22 M. Cossi and V. Barone, *J. Chem. Phys*, 2000, **112**, 2427–2435.

23 M. Cossi, G. Scalmani, N. Rega and V. Barone, *J. Chem. Phys.*, 2002, **117**, 43–54.
24 F. Aquilante, V. Barone and B. O. Roos, *J. Chem. Phys.*, 2003, **119**, 12323–12334.
25 M. J. Frisch, G. W. Trucks, H. B. Schlegel, G. E. Scuseria, M. A. Robb, J. R. Cheeseman, J. A. Montgomery Jr., T. Vreven, K. N. Kudin, J. C. Burant, J. M. Millam, S. S. Iyengar, J. Tomasi, V. Barone, B. Mennucci, M. Cossi, G. Scalmani, N. Rega, G. A. Petersson, H. Nakatsuji, M. Hada, M. Ehara, K. Toyota, R. Fukuda, J. Hasegawa, M. Ishida, T. Nakajima, Y. Honda, O. Kitao, H. Nakai, M. Klene, X. Li, J. E. Knox, H. P. Hratchian, J. B. Cross, C. Adamo, J. Jaramillo, R. Gomperts, R. E. Stratmann, O. Yazyev, A. J. Austin, R. Cammi, C. Pomelli, J. W. Ochterski, P. Y. Ayala, K. Morokuma, G. A. Voth, P. Salvador, J. J. Dannenberg, V. G. Zakrzewski, S. Dapprich, A. D. Daniels, M. C. Strain, O. Farkas, D. K. Malick, A. D. Rabuck, K. Raghavachari, J. B. Foresman, J. V. Ortiz, Q. Cui, A. G. Baboul, S. Clifford, J. Cioslowski, B. B. Stefanov, G. Liu, A. Liashenko, P. Piskorz, I. Komaromi, R. L. Martin, D. J. Fox, T. Keith, M. A. Al-Laham, C. Y. Peng, A. Nanayakkara, M. Challacombe, P. M. W. Gill, B. Johnson, W. Chen, M. W. Wong, C. Gonzalez and J. A. Pople, *GAUSSIAN 03 (Revision B.05)*, Gaussian, Inc., Pittsburgh, PA, 2003.
26 M. A. Aguilar, F. J. Olivares del Valle and J. Tomasi, *J. Chem. Phys.*, 1993, **98**, 7375–7384.
27 B. Mennucci, R. Cammi and J. Tomasi, *J. Chem. Phys.*, 1998, **109**, 2798–2807.
28 *Chemical Applications of Density Functional Theory*, ed. E. J. Baerends, O. V. Gritsenko and R. van Leeuwen, ACS Symposium Series No. 269, American Chemical Society, 1996, vol. **20**, pp. 20–35.
29 R. Stowasser and R. Hoffmann, *J. Am. Chem. Soc.*, 1999, **121**, 3414–3420.
30 V. Barone, O. Crescenzi and R. Improta, *Quant. Struct.-Act. Relat.*, 2002, **21**, 105–118.
31 W. A. Case and D. R. Kearns, *J. Chem. Phys.*, 1970, **52** 2175–2191.
32 K. Ravikumar, *Acta Crystallogr., Sect. C*, 1994, **50**, 589–592.
33 A. Dreuw and M. Head-Gordon, *J. Am. Chem. Soc.*, 2004, **126**, 4007–4016.
34 S. Grimme and M. Parac, *ChemPhysChem.*, 2003, **4**, 292–295.
35 M. Cossi and V. Barone, *J. Chem. Phys*, 2001, **115**, 4708–4717.
36 C.-G. Zhan, J. A. Nichols and D. A. Dixon, *J. Phys. Chem. A*, 2003, **107**, 4183–4195.
37 T. P. Straatsma, E. Aprà, T. L. Windus, E. J. Bylaska, W. de Jong, S. Hirata, M. Valiev, M. T. Hackler, L. Pollack, R. J. Harrison, M. Dupuis, D. M. A. Smith, J. Nieplocha, V. Tipparaju, M. Krishnan, A. Auer, E. Brown, G. Cisneros, G. I. Fann, H. Fruchtl, J. Garza, K. Hirao, R. Kendall, J. Nichols, K. Tsemekhman, K. Wolinski, J. Anchell, D. Bernholdt, P. Borowski, T. Clark, D. Clerc, H. Dachsel, M. Deegan, K. Dyall, D. Elwood, E. Glendening, M. Gutowski, A. Hess, J. Jaffe, B. Johnson, J. Ju, R. Kobayashi, R. Kutteh, Z. Lin, R. Littlefield, X. Long, B. Meng, T. Nakajima, S. Niu, M. Rosing, G. Sandrone, M. Stave, H. Taylor, G. Thomas, J. van Lenthe, A. Wong and Z. Zhang, *NWChem, a Computational Chemistry Package for Parallel Computers*, Version 4.6, Pacific Northwest National Laboratory, Richland, WA, 2004.
38 R. J. Cave, K. Burke, Jr. and E. W. Castner, *J. Phys. Chem. A*, 2002, **106**, 9294–9305.
39 M. E. Casida, F. Gutierrez, J. Guan, F. X. Gadéa, D. Salahub and J.-P. Daudey, *J. Chem. Phys*, 2000, **113**, 7062–7071.